Boundary Layer Stability Analysis for Stetson's Mach 6 Blunt Cone Experiments

Joseph S. Jewell* and Roger L. Kimmel†

U.S. Air Force Research Laboratory, WPAFB, OH 45433, USA

The results of a seminal experimental study of the effects of bluntness and swallowing length on transition on an 8-degree cone at zero angle of attack in Mach 6 high Reynolds number flow are analyzed with the STABL computational fluid dynamics code package. Mean flow solutions and PSE-Chem stability analyses for a total of 11 different nose tip bluntnesses, ranging from sharp to 15.24 mm radius, are obtained. For the sharpest cases, $N_{Tr} \approx 7$, but as bluntness increases and the calculated swallowing distance lengthens, the computed N-factor at the experimentally-observed transition location drops below the level at which Mack's second mode would be expected to lead to transition. These results indicate that the dominant instability mechanism for the bluntest cases is not the second mode.

I. Introduction

Boundary layer transition is a critical factor in the design of hypersonic vehicles, with profound impact on both heat transfer and control characteristics. While many practical aerospace vehicles are blunt, the mechanisms that lead to boundary layer instability and transition on sharp bodies are more thoroughly understood at present. However, over the past half century, a wealth of relevant wind tunnel and flight data has been acquired. Analytical and computational techniques, as well as the rapid development of economical and powerful computer processors, have made possible comprehensive computational analysis of existing experimental data sets.

Between 1978 and 1982, K. F. Stetson performed a total of 196 sharp- and blunt-cone experiments[1] on an 8-degree half-angle, 4 in.-base cone in the Air Force Research Laboratory Mach 6 High Reynolds Number facility. These experiments were reported in a 1983 paper[2] along with results from AEDC Tunnel F with a larger cone at Mach 9. While the AEDC Mach 9 results have received computational analysis,[3] the AFRL Mach 6 results have not, to date.

The AFRL Mach 6 facility operates at stagnation pressure p_0 from 700 to 2100 psi. Details of these conditions, along with an intermediate case, are presented in Table 1. A total of 196 experiments[1] encompassing 108 unique conditions comprise the Stetson[2] Mach 6 results (see Section III). Mean-flow and stability calculations for each unique condition were performed at a computational cost of about 100 processor-hours each.

Table 1. Summary of sample inflow conditions computed for each bluntness value, with one intermediate value presented. These conditions encompass the operating envelope of the AFRL Mach 6 High Reynolds Number facility.

p_0		unit Re_∞	M_∞	ρ_∞	P_∞	T_∞	U_∞	T_w/T_0
[psi]	[MPa]	$\times 10^6$/m	-	[kg/m3]	[kPa]	[K]	[m/s]	-
700	4.83	30.7	5.9	0.154	3.40	76.7	1038	0.56
1400	9.65	61.4	5.9	0.308	6.80	76.7	1038	0.56
2100	14.5	92.1	5.9	0.461	10.2	76.7	1038	0.56

*Research Aerospace Engineer (NRC Research Associate), AFRL/RQHF, Wright-Patterson AFB, OH 45433. AIAA Senior Member. jjewell@alumni.caltech.edu

†Principal Aerospace Engineer, AFRL/RQHF, Wright-Patterson AFB, OH 45433. AIAA Associate Fellow.

American Institute of Aeronautics and Astronautics
Cleared for Public Release, Case Number: 88ABW-2015-5892.

II. Computational Methods

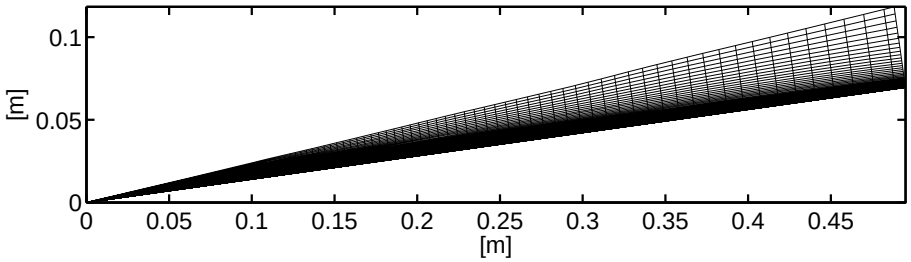

Figure 1. Grid for the sharp cone case with 361 streamwise and 359 wall-normal cells. For clarity, every fifth wall-normal cell is shown.

The mean flow over the cone is computed by the reacting, axisymmetric Navier-Stokes equations with a structured grid, using a version of the NASA Data Parallel-Line Relaxation (DPLR) code[4] which is included as part of the STABL software suite, as described by Johnson[5] and Johnson et al.[6] This flow solver is based on the finite-volume formulation. The use of an excluded volume equation of state is not necessary for the boundary layer solver because the static pressure over the cone is sufficiently low (typically, 10–50 kPa) that the gas can be treated as ideal. The mean flow is computed on a single-block, structured grid (see Figure 1) with dimensions of 361 cells by 359 cells in the streamwise and wall-normal directions, respectively. The inflow gas composition in each case is air with 0.233 O_2 and 0.767 N_2 mass fractions. While the computation includes chemistry, the impact of chemical reactions is negligible, as the local maximum temperature does not exceed 611 K for any case.

Grids for the sharp 8-degree half angle cone and each of the 10 bluntness conditions (see Table 2) were generated using STABL's built-in grid generator, and mean flow solutions examined to ensure that at least 100 points were placed in the boundary layer for each stagnation pressure. The boundary-layer profiles and edge properties are extracted from the mean flow solutions during post-processing. The wall-normal span of the grid increases down the length of the cone, from 0.25 mm at the tip to 50 mm at the base, allowing for the shock to be fully contained within the grid for all cases tested. The grid is clustered at the wall as well as at the nose in order to capture the gradients in these locations. The Δy^+ value for the grid, extracted from the DPLR solution for each case, is everywhere less than 1, where Δy^+ is a measure of local grid quality at the wall in the wall-normal direction.

Table 2. Summary of grids generated for the present study, each corresponding to a different sharp or blunt nose tip used by Stetson.[2] For simplicity and to match the Stetson nomenclature, bluntness as a percentage of the base radius of 2.0 inches is used to label the cases analyzed in the present work.

R_N		Bluntness
in.	mm	%
0	0	0
0.02	0.508	1
0.04	1.016	2
0.06	1.524	3
0.08	2.032	4
0.10	2.540	5
0.20	5.080	10
0.30	7.620	15
0.40	10.16	20
0.50	12.70	25
0.60	15.24	30

III. Mean Flow-Based Transition Correlations

Stetson[2] reported results by "normalizing" the transition Reynolds numbers for blunted cones by the transition Reynolds numbers for sharp cones at the same inflow conditions, which are calculated as:

$$\frac{X_{\mathrm{Tr_B}}}{X_{\mathrm{Tr_S}}} = \frac{(\mathrm{Re}_{X_e})_{\mathrm{Tr_B}}}{(\mathrm{Re}_{X_e})_{\mathrm{Tr_S}}} \frac{(\mathrm{Re_{unit}})_{\mathrm{e_S}}}{(\mathrm{Re_{unit}})_{\mathrm{e_B}}}$$

Here, subscript "S" indicates values for a sharp tip, "B" values for a given blunt tip at the same condition, and "e" conditions at the boundary layer edge. The boundary layer edge, throughout the present work, is defined as the point at which the derivative of the enthalpy along a line extending orthogonally from the surface of the cone approaches zero. Stetson[2] performed selected computations with two boundary layer codes and used some interpolations to find the unit Reynolds number and Mach number at the boundary layer edge and throughout the entropy layer, but notes that "it was not considered practical to make boundary layer calculations for all of the geometric and flow variations of the present investigation." This is now possible; two examples for a sharp and blunt case are presented in Figure 2.

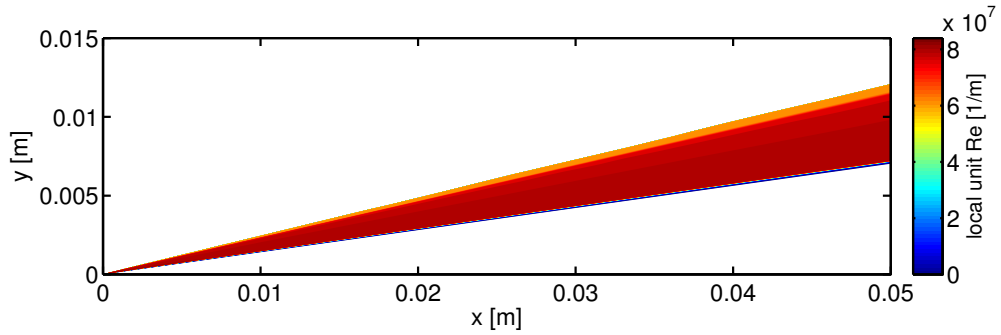

(a) Sharp tip

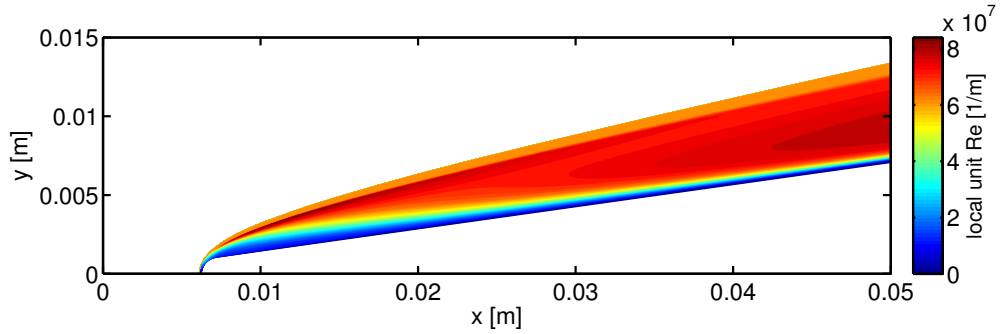

(b) R_N = 1.016 mm (2%)

Figure 2. Sharp and blunt unit Reynolds number contours (detail, first 5 cm of the cone) for the p_0 = 1400 psi inflow case. While the freestream unit Reynolds number is 61.4×10^6/m for both cases, the large "swallowing length" of the blunt case is evident as a large local region of low unit Reynolds number fluid behind the curved shock and next to the wall, approximately coincident with the high entropy region depicted in Figure 3.

The entropy layer swallowing length estimate of Rotta[7] (X_{SW}), as applied by Stetson and Rushton,[8] is also used to correlate the results. The entropy layer is depicted directly by using the DPLR solution for each case (gas composition, temperature, and pressure) as the input for an entropy calculation at each cell, which is performed using the Cantera[9] thermodynamics software and presented in Figure 3 for a sharp and blunt case.

Figure 9 in Stetson[2] summarizes his results, and is recreated using the transition locations reported in Stetson,[1] but with the present condition computations, below as Figures 4 and 5.

Following Marineau et al.[10] and Moraru,[11] the Stetson[2] results may also be presented, as in Figure 6, as a function of the freestream Reynolds number calculated with the nose radius as the relevant length scale.

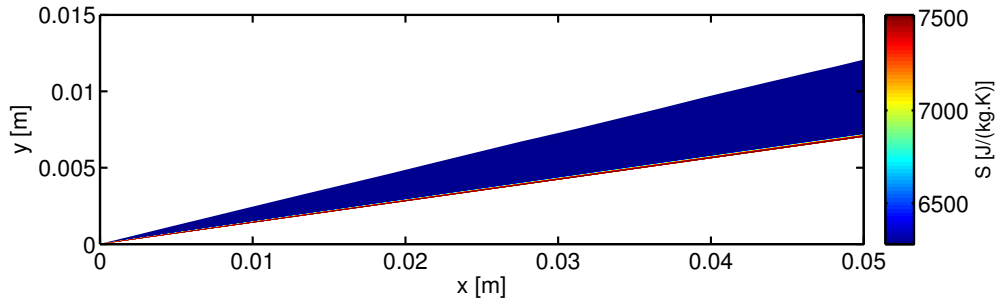

(a) Sharp tip

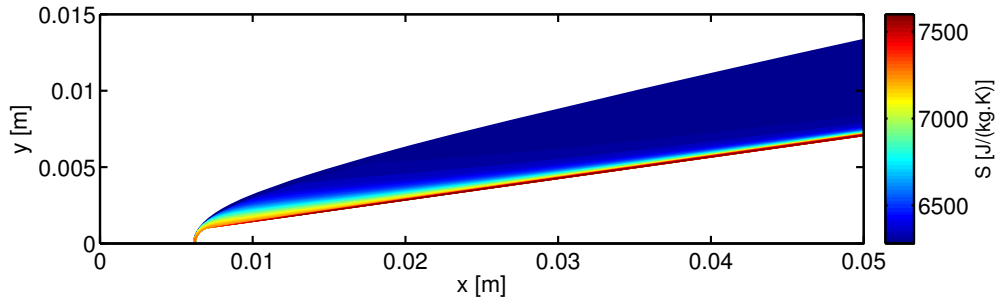

(b) R_N = 1.016 mm (2%)

Figure 3. Sharp and blunt entropy contours (detail, first 5 cm of the cone) for the p_0 = 1400 psi inflow case. The large entropy layer "swallowing length" of the blunt case is evident as a large local region of high entropy fluid behind the curved shock and next to the wall, which is initially much thicker than the boundary layer. The estimated swallowing length X_{SW} calculated with the method of Rotta[7] as applied by Stetson and Rushton[8] is 24.2 cm for this case, well beyond the field of view for this plot.

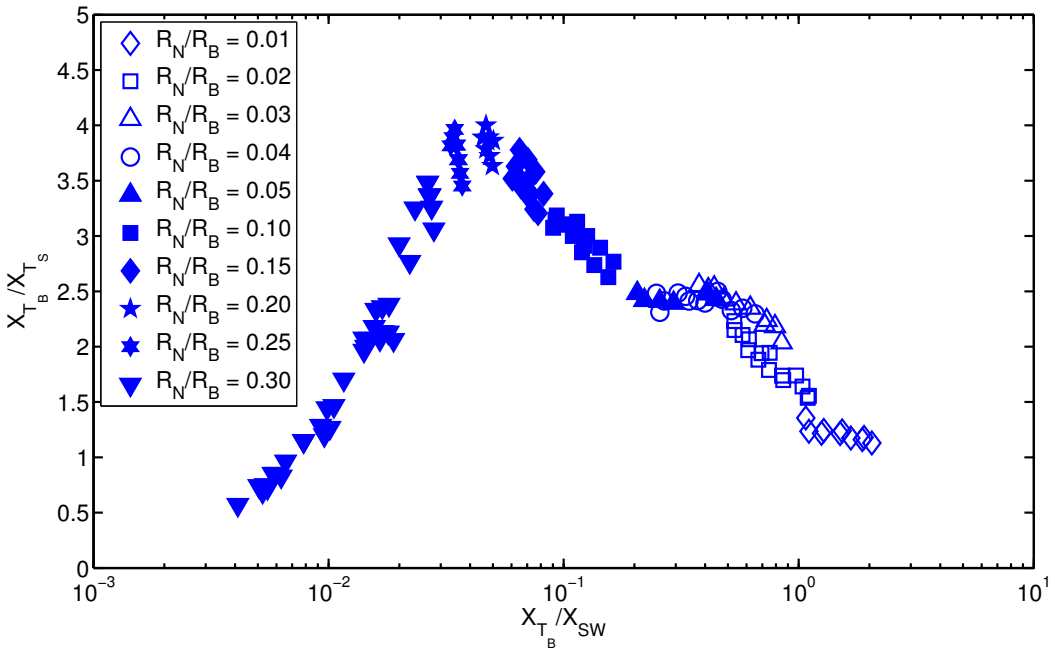

Figure 4. Stetson[2] Figure 9(a). Effect of nosetip bluntness (normalized by the swallowing length of Rotta[7] in terms of the transition location ratio.

In this approach, the freestream Reynolds number at observed transition location increases with nosetip Reynolds number before dropping off sharply at about 9×10^5. This pattern is consistent with that observed by Marineau et al.[10] and Moraru,[11] although those authors found the dropoff point at nosetip Reynolds numbers of about 3×10^5. A similar plot, with the transition Reynolds number calculated with the conditions

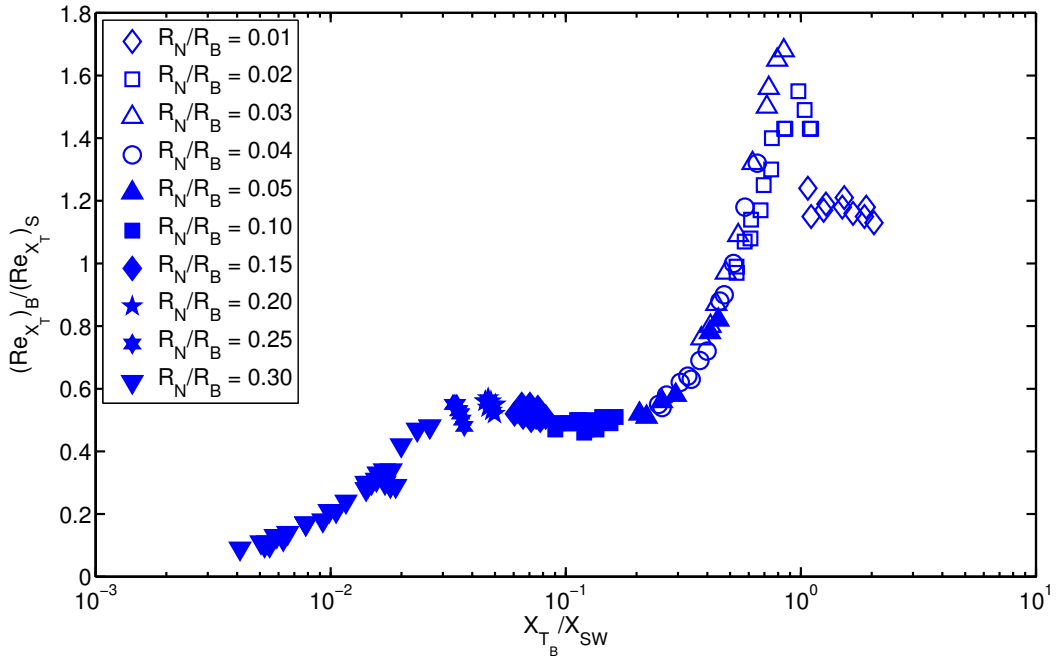

Figure 5. Stetson[2] Figure 9(b). Effect of nosetip bluntness (normalized by the swallowing length of Rotta[7] in terms of the transition Reynolds number ratio.

at the edge of the boundary layer at the transition onset location instead of from the freestream, is presented in Figure 7.

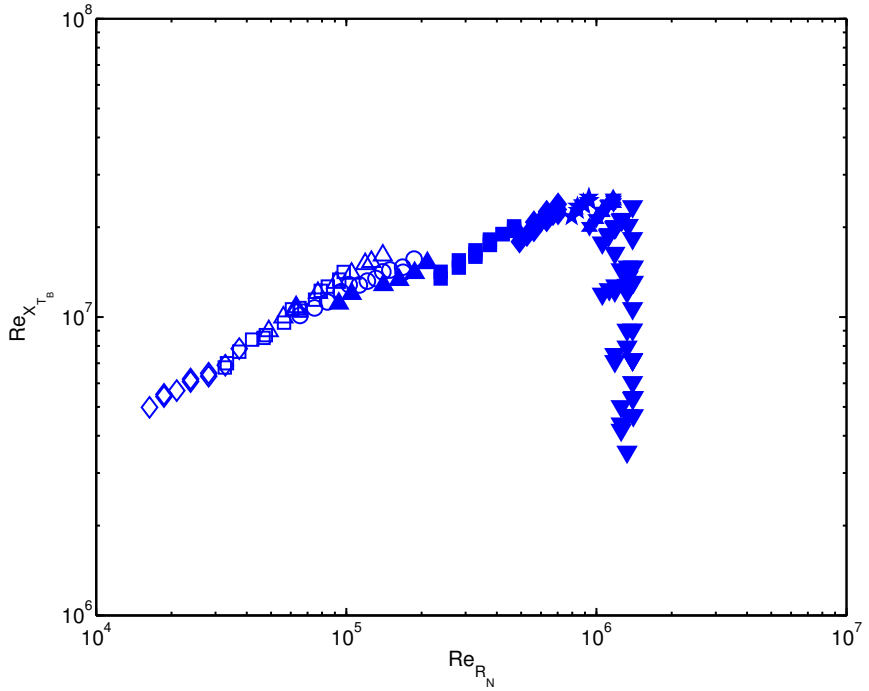

Figure 6. Stetson[2] results as a function of nosetip Reynolds number. Both Reynolds numbers in this plot are calculated at freestream conditions.

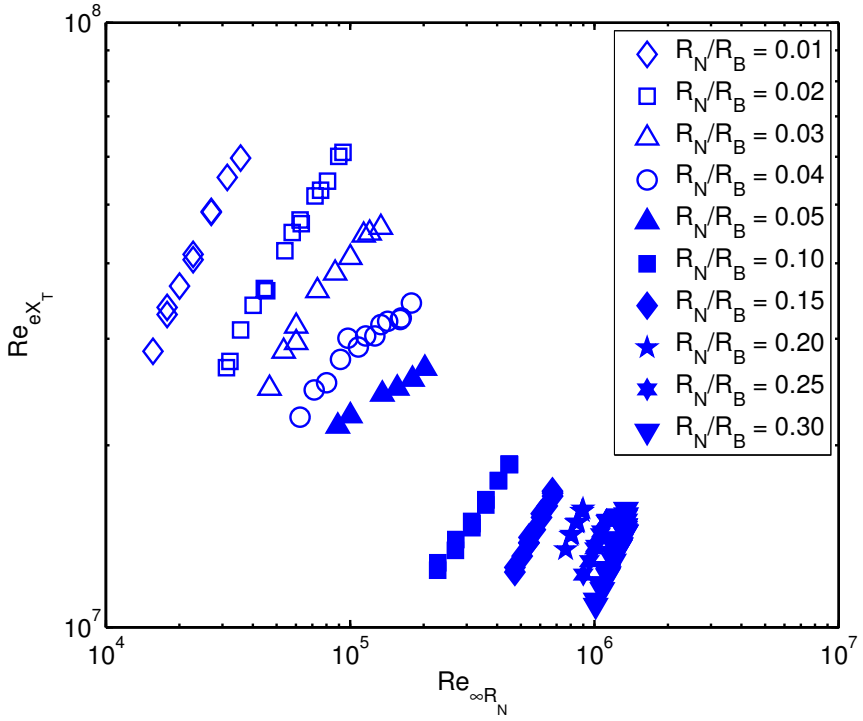

Figure 7. Stetson[2] results as a function of nosetip Reynolds number. The nose Reynolds numbers in this plot is calculated with freestream conditions, and the transition Reynolds number is calculated with the conditions at the edge of the boundary layer at the transition onset location.

IV. Stability Computations

The stability analyses are performed using the PSE-Chem solver, which is also part of the STABL software suite. PSE-Chem[12] solves the reacting, two-dimensional, axisymmetric, linear parabolized stability equations (PSE) to predict the amplification of disturbances as they interact with the boundary layer. The PSE-Chem solver includes finite-rate chemistry and translational-vibrational energy exchange. The parabolized stability equations predict the amplification of disturbances as they interact with the boundary layer.

The band of amplified frequencies within the boundary layer predicted by Linear Stability Theory (LST) is presented in a contour plot in terms of amplification $-\alpha_i$ in Figure 8. The most amplified frequency predicted by a simple model based on edge velocity and boundary layer thickness is also plotted, and shows generally good agreement with the detailed computations.

In the present work the focus was on the 2D second mode, which should be dominant above approximately Mach 4.5[13] for conical geometry with significant wall cooling. Frequencies low enough to include the 2D first mode were also examined comprehensively, and oblique first modes were included in the computation for a few of the blunt cases, but significant amplification was not observed in the computational results for any of these. Marineau et al.[10] also did not observe strong first-mode activity in experimental results derived from a ray of surface mounted pressure transducers. Nevertheless, for the present data set, future work should include a more systematic look at oblique first modes to confirm their exclusion as the dominant instability mechanism for the blunt cases.

Computed second mode N-factors at the experimental transition location are presented in Figure 9. An inset plot details the region of most rapid change in transition N-factor. Three regions are evident: for $X_T/X_{SW} < 0.3$, the computed N-factors at transition are less than one, indicating that modal growth is minimal and implying that an alternate transition mechanism is important in this region, which is populated by the blunter cases. Marineau et al.,[10] who observed a similar effect, propose that transient growth[14] or entropy-layer instability[15] may be plausible candidate mechanisms. From $0.3 < X_T/X_{SW} < 1.0$, the computed N-factor of transition rapidly increases. In this region, significant modal growth occurs and may compete

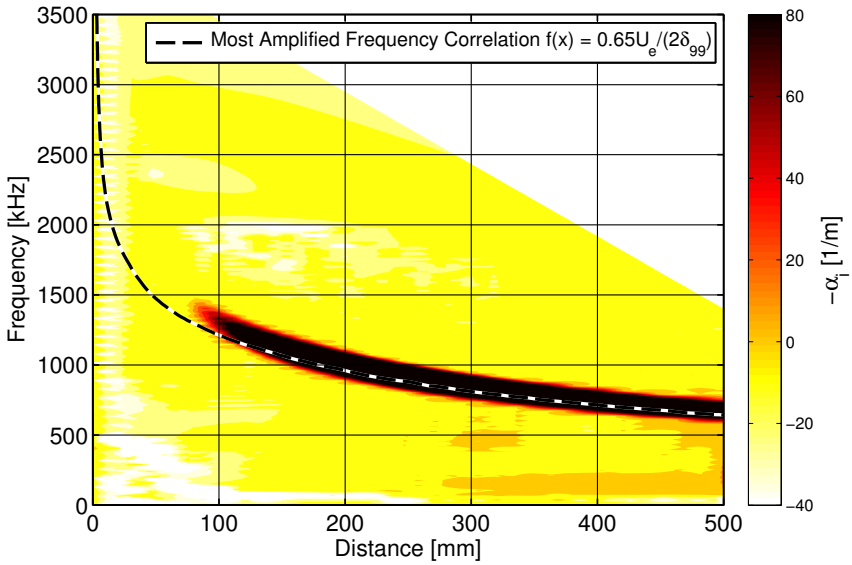

Figure 8. LST contours of $-\alpha_i$ for $R_N = 1.016$ mm (2%) for the $p_0 = 1400$ psi inflow condition, showing good agreement with a simple frequency correlation for this mildly-blunt case.

with other mechanisms to provoke laminar-turbulent transition. For $X_T/X_{SW} > 1.0$, which includes the sharpest cones in the data set, a consistent computed transition N-factor, falling within a range of 6.9 to 7.7, is observed. This result is consistent with Mack's second mode[13] as the dominant instability mechanism for the sharpest cases.

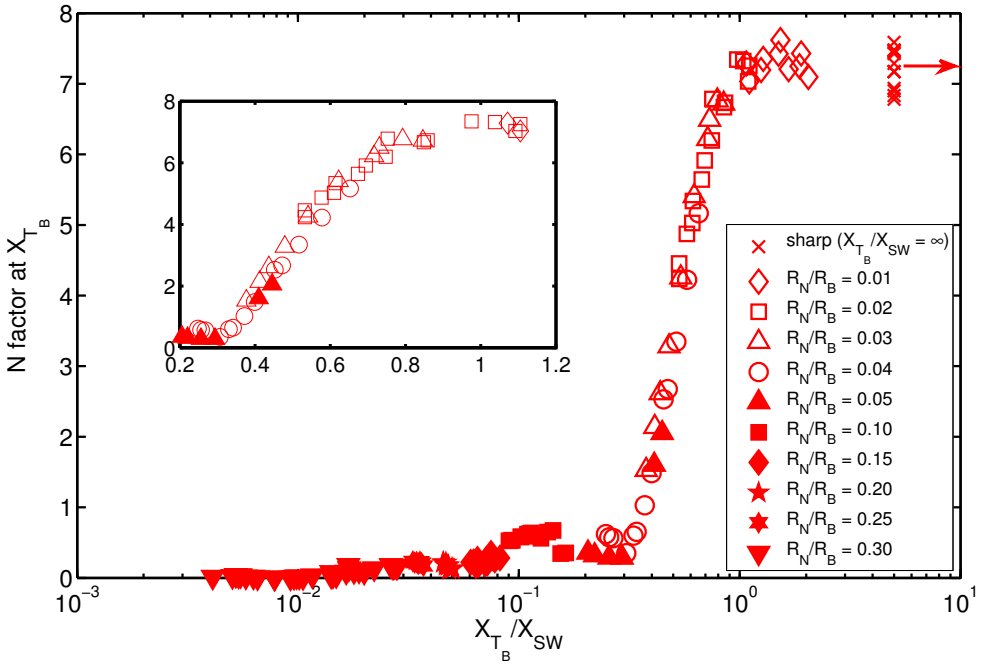

Figure 9. Computed N-factor at experimental transition location reported in Stetson.[1,2] A strong trend with both nose tip bluntness and swallowing length ratio is observed. Note that the sharp data points (noted with an arrow) are located at infinity on the x-axis, as the swallowing length approaches infinity, and appear to be the asymptotic value for N-factor at transition with decreasing nose tip bluntness. The inset plot details the region of most rapid change in transition N-factor.

Transition in conventional hypersonic wind tunnels on cones with small bluntness has in some cases[16] been well-correlated with N-factors of about 5.5. Recent results[17–20] have found higher transition N-factors in noisy

hypersonic tunnels for cases where there is a mismatch between the strongest free stream noise frequencies and the most unstable boundary-layer frequencies. Evidence supporting this mismatch hypothesis in previous studies has included a dependency of the correlating N-factor with the most unstable frequency at transition, in an effort to account for decreasing tunnel noise amplitude at higher frequencies. In contrast, the present data does not show any obvious systematic variation in computed most amplified frequency at the measured transition location. Figure 10, which shows the calculated most-amplified frequency at transition, has the same x-axis (X_T/X_{SW}) as Figure 9. There is no obvious correlation between the most amplified frequency at transition and the N-factor at transition in this coordinate system.

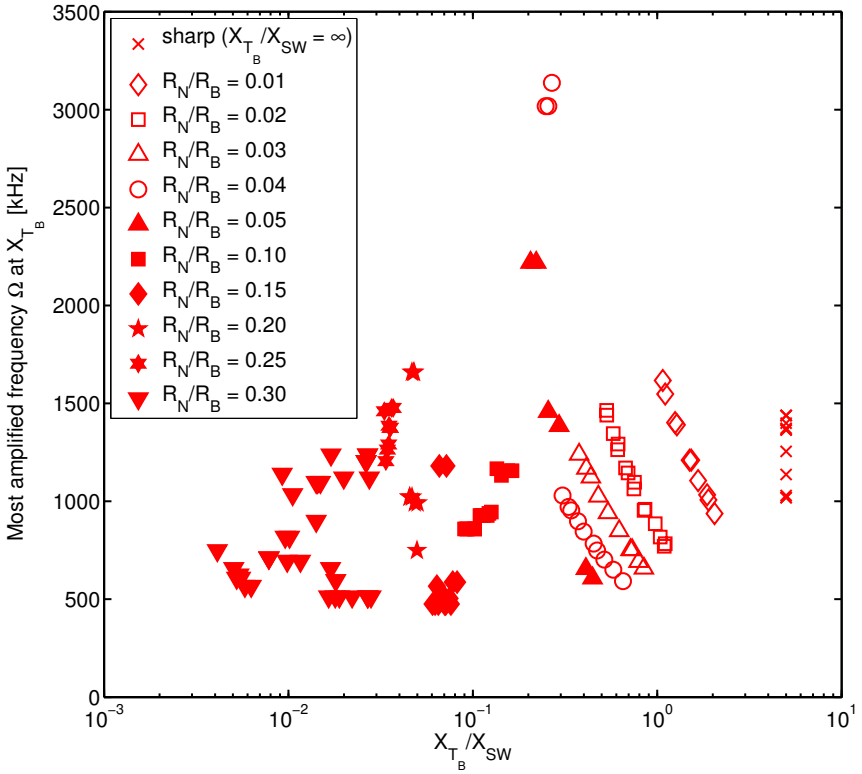

Figure 10. Computed most amplified frequency at the measured transition location. No systematic variation in X_T/X_{SW} is observed. The outliers above 2000 kHz are likely the result of early bypass transition in the associated experiments, caused by roughness, particulate, or another unknown factor, when the boundary layer is still relatively thin and the calculated most unstable frequency is therefore large.

The region in which the second mode is significant may be defined by Mach number at the boundary layer edge, which in Figure 11a is presented at the measured point of transition as a function of X_T/X_{SW}. Figure 11b presents the variation of computed N-factor at the measured transition location as a function of edge Mach number. The maximum computed second mode N-factors occur for $M_e > 4.5$, while small second mode N-factors are computed for $M_e < 3.9$, which is consistent with the predictions of Mack[13] for the variation in the strength of the second-mode instability with Mach number. As bluntness and resultant entropy layer swallowing length effectively mediate the edge Mach number, this may be the effect by which the second mode is emphasized or de-emphasized in the transition process, but it does not indicate the alternate mechanism for instability which is important in the blunter cases with lower edge Mach number. While preliminary first mode analysis has not shown significant amplification, future work should include a more systematic look at oblique first modes to confirm their exclusion as the dominant instability mechanism for the blunt cases.

V. Conclusions

A strong trend in transition N-factor for both nose tip bluntness and swallowing length ratio is observed in the results computed (see Figure 9) from the complete set of Stetson[2] Mach 6 conditions. As bluntness increases and the calculated swallowing distance lengthens, the computed N-factor at the experimentally-

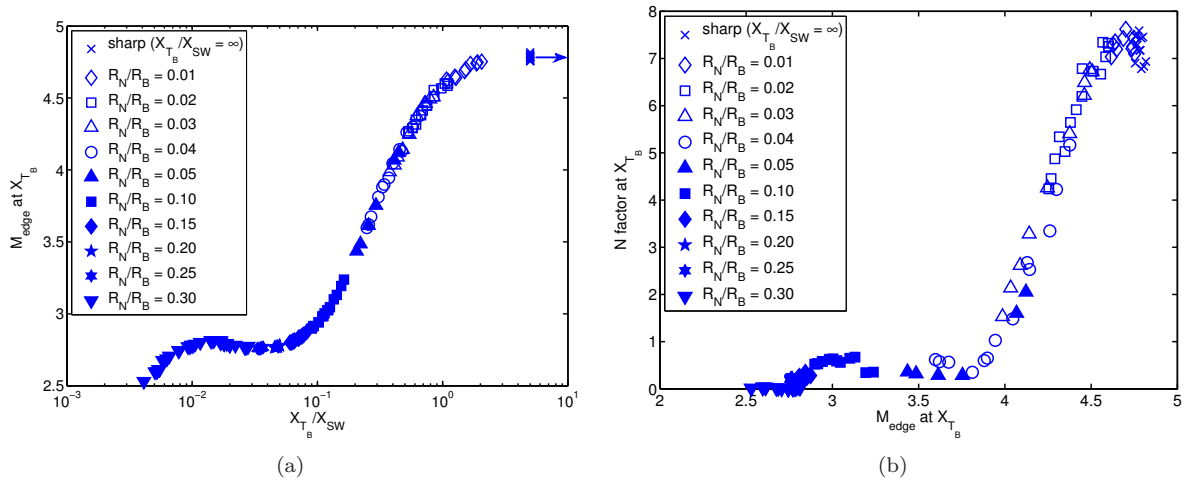

(a) (b)

Figure 11. Edge Mach number effects in the present data set. In a), Mach number at the boundary layer edge at the measured point of transition is shown as a function of X_T/X_{SW}. In b), the variation of computed N-factor at the measured transition location is shown as a function of edge Mach number.

observed transition location drops below the level at which Mack's second mode[13] would be expected to lead to transition.[21,22] These results indicate that the dominant instability mechanism for the bluntest cases is likely not the second mode, which is consistent with recent blunt cone results[10] at different conditions. Alternate instability mechanisms include transient growth[14] and entropy-layer instability.[15]

Based upon the computed second-mode amplification factors e^N, transition onset in the AFRL Mach 6 High Reynolds Number facility is estimated to correspond to N ≈ 7 for the sharp and nearly sharp cases. These amplification values are high as compared to the more typical value of N ≈ 5–6 usually characterizing a "noisy" tunnel.[23] One partial explanation may be a mismatch between the strongest free stream noise frequencies and the most unstable second mode boundary-layer frequencies; however, no systematic variation in the computed most-unstable frequency at observed transition location is seen in the present data set. Measurements of free stream and boundary layer instabilities in the Mach 6 tunnel, as well as further analysis of the oblique first modes, would be essential for further investigation of this potential effect.

Acknowledgments

The authors thank Prof. Steve Schneider of Purdue for sharing his private communication with Ken Stetson,[1] which provided additional clarification, and tabulated data, for the results reported in Stetson's 1983 paper on Mach 6 blunt cone experiments,[2] and Dr. Eric Marineau of AEDC for helpful discussion. J. S. Jewell thanks Dr. Ross Wagnild of Sandia for his patient advice on the use of the STABL code. This research was performed while J. S. Jewell held a National Research Council Research Associateship Award at the Air Force Research Laboratory.

References

[1]Stetson, K. F., "Notes related to previous AIAA papers on blunt cones," Personal communication to S. P. Schneider, December 2001, Purdue University.

[2]Stetson, K. F., "Nosetip Bluntness Effects on Cone Frustum Boundary Layer Transition in Hypersonic Flow," *Proceedings of the AIAA 16th Fluid and Plasma Dynamics Conference*, AIAA-83-1763, Danvers, Massachusetts, 1983.

[3]Robarge, T. W. and Scheider, S. P., *Laminar boundary-layer instabilities on hypersonic cones: Computations for benchmark experiments*, AIAA-2005-5024, Toronto, ON, 2005.

[4]Wright, M. J., Candler, G. V., and Bose, D., "Data-parallel line relaxation method for the Navier-Stokes equations," *AIAA Journal*, Vol. 36, No. 9, 1998, pp. 1603–1609.

[5]Johnson, H. B., *Thermochemical Interactions in Hypersonic Boundary Layer Stability*, Ph.D. thesis, University of Minnesota, Minneapolis, MN, 2000.

[6]Johnson, H. B., Seipp, T. G., and Candler, G. V., "Numerical study of hypersonic reacting boundary layer transition on

cones," *Physics of Fluids*, Vol. 10, 1998, pp. 2676–2685.

[7]Rotta, N. R., "Effects of nose bluntness on the boundary layer characteristics of conical bodies at hypersonic speeds," New York University Report NYUAA-66-66, 1966.

[8]Stetson, K. F. and Rushton, G. H., "Shock Tunnel Investigation of Boundary-Layer Transition at M = 5.5," *AIAA Journal*, Vol. 5, No. 5, 1967, pp. 899–906.

[9]Goodwin, D., "Cantera: An object-oriented software toolkit for chemical kinetics, thermodynamics, and transport processes," Available: http://code.google.com/p/cantera, 2009, Accessed: 12/12/2012.

[10]Marineau, E. C., Moraru, C. G., Lewis, D. R., Norris, J. D., Lafferty, J. F., Wagnild, R. M., and Smith, J. A., "Mach 10 boundary-layer transition experiments on sharp and blunted cones," *Proceedings of 19th AIAA International Space Planes and Hypersonic Systems and Technologies Conference*, AIAA-2014-3108, Atlanta, GA, 2014.

[11]Moraru, C. G., *Hypersonic boundary-layer transition measurements at Mach 10 on a large seven-degree cone at angle of attackr*, Master's thesis, Purdue University, 2015.

[12]Johnson, H. B. and Candler, G. V., "Hypersonic boundary layer stability analysis using PSE-Chem," *35th Fluid Dynamics Conference and Exhibit*, AIAA, 2005, AIAA-2005-5023.

[13]Mack, L. M., "Boundary-layer linear stability theory. special course on stability and transition of laminar flow advisory group for aerospace research and development," Tech. rep., 1984, AGARD Report No. 709.

[14]Reshotko, E., "Transient growth: A factor in bypass transition," *Physics of Fluids*, Vol. 13, No. 5, 2001, pp. 1067–1075.

[15]Kufner, E. and Dallmann, U., "Entropy-and Boundary Layer Instability of Hypersonic Cone Flows-Effects of Mean Flow Variations," *Laminar-Turbulent Transition*, Springer, 1995, pp. 197–204.

[16]Alba, C. R., Johnson, H. B., Bartkowicz, M. D., Candler, G. V., and Berger, K. T., "Boundary-layer stability calculations for the HIFiRE-1 transition experiment," *Journal of Spacecraft and Rockets*, Vol. 45, No. 6, 2008, pp. 1125–1133.

[17]Jewell, J. S., Wagnild, R. M., Leyva, I. A., Candler, G. V., and Shepherd, J. E., "Transition Within a Hypervelocity Boundary Layer on a 5-Degree Half-Angle Cone in Air/CO_2 Mixtures," *51st AIAA Aerospace Sciences Meeting including the New Horizons Forum and Aerospace Exposition*, AIAA-2013-0523, Grapevine, TX, 2013.

[18]Jewell, J. S., *Boundary-Layer Transition on a Slender Cone in Hypervelocity Flow with Real Gas Effects*, Ph.D. thesis, California Institute of Technology, Pasadena, CA, 2014.

[19]Parziale, N. J., Jewell, J. S., Leyva, I. A., and Shepherd, J. E., "Effects of Shock-Tube Cleanliness on Slender-Body Hypersonic Instability and Transition Studies at High Enthalpy," *Proceedings of 53rd AIAA Aerospace Sciences Meeting*, AIAA-2015-1786, Orlando, FL, 2015.

[20]Jewell, J. S., Parziale, N. J., Leyva, I. A., and Shepherd, J. E., "Effects of Shock-Tube Cleanliness on Slender-Body Hypersonic Instability and Transition Studies at High Enthalpy," Submitted, 2016.

[21]Fedorov, A. V., "Receptivity of a High-Speed Boundary Layer to Acoustic Disturbances," *Journal of Fluid Mechanics*, Vol. 491, 2003, pp. 101–129.

[22]Fedorov, A. and Tumin, A., "High-Speed Boundary-Layer Instability: Old Terminology and a New Framework," *AIAA Journal*, Vol. 49, 2011, pp. 1647–1657.

[23]Schneider, S. P., "Effects of High-Speed Tunnel Noise on Laminar-Turbulent Transition," *Journal of Spacecraft and Rockets*, Vol. 38, No. 3, 2001, pp. 323–333.